

Site occupancy and magnetic properties of Al-substituted M-type strontium hexaferrite

Vivek Dixit, Chandani N. Nandadasa, and Seong-Gon Kim*

*Department of Physics and Astronomy, Mississippi State University, Mississippi State, MS 39762, USA and
Center for Computational Sciences, Mississippi State University, Mississippi State, MS 39762, USA*

Sungho Kim

Center for Computational Sciences, Mississippi State University, Mississippi State, MS 39762, USA

Jihoon Park and Yang-Ki Hong

*Department of Electrical and Computer Engineering and MINT Center,
The University of Alabama, Tuscaloosa, AL 35487, USA*

Laalitha S. I. Liyanage

Department of Physics, University of North Texas, Denton, TX 76203, USA

Amitava Moitra

*Thematic Unit of Excellence on Computational Materials Science,
S.N. Bose National Centre for Basic Sciences, Sector-III, Block-JD, Salt Lake, Kolkata-700098, India*

(Dated: April 6, 2015)

We use first-principles total-energy calculations based on density functional theory to study the site occupancy and magnetic properties of Al-substituted M-type strontium hexaferrite $\text{SrFe}_{12-x}\text{Al}_x\text{O}_{19}$ with $x = 0.5$ and $x = 1.0$. We find that the non-magnetic Al^{3+} ions preferentially replace Fe^{3+} ions at two of the majority spin sites, $2a$ and $12k$, eliminating their positive contribution to the total magnetization causing the saturation magnetization M_s to be reduced as Al concentration x is increased. Our formation probability analysis further provides the explanation for increased magnetic anisotropy field when the fraction of Al is increased. Although Al^{3+} ions preferentially occupy the $2a$ sites at a low temperature, the occupation probability of the $12k$ site increases with the rise of the temperature. At a typical annealing temperature ($> 700^\circ\text{C}$) Al^{3+} ions are much more likely to occupy the $12k$ site than the $2a$ site. Although this causes the magnetocrystalline anisotropy K_1 to be reduced slightly, the reduction in M_s is much more significant. Their combined effect causes the anisotropy field H_a to increase as the fraction of Al is increased, consistent with recent experimental measurements.

I. INTRODUCTION

Strontium hexaferrite, $\text{SrFe}_{12}\text{O}_{19}$ (SFO) is one of the most commonly used materials for permanent magnets, magnetic recording and data storage, and components in electrical devices operating at microwave/GHz frequencies, due to its high Curie temperature, large saturation magnetization, excellent chemical stability and low manufacturing cost [1–5]. However, in comparison with Nd-Fe-B and magnet, the coercivity of the SFO is low and presents a significant limitation in its application. Therefore, enhancement of the coercivity is an important research topic for the strontium hexaferrite.

In order to tailor the magnetic properties such as magnetization and coercivity, various cation substitutions in the M-type hexaferrites have been investigated. For example, the substitution of La [6, 7], Sm [8], Pr [9] and Nd [10] in the SFO increased coercivity moderately while the substitution of Zn-Nb [11], Zn-Sn [12–14] and Sn-Mg

[4] decreased coercivity. However, the coercivity of the M-type hexaferrites is not increased significantly by these cation substitutions, and is still much smaller than that of Nd-Fe-B magnet [15].

Al substitution in the M-type hexaferrite has been more effective in enhancing coercivity [16–20]. Particularly, Wang et al synthesized Al-doped SFO $\text{SrFe}_{12-x}\text{Al}_x\text{O}_{19}$ (SFAO) with Al content of $x = 0 - 4$ using glycinnitrate method and subsequent annealing in a temperature over 700°C obtaining the largest coercivity of 17.570 kOe, which is much larger than that of SFO (5.356 kOe) and exceeds even the coercivity of the $\text{Nd}_2\text{Fe}_{17}\text{B}$ (15.072 kOe) [1]. Wang and co-workers also observed that the coercivity of the SFAO increases with increasing Al concentration at a fixed annealing temperature. These results call for a systematic understanding, from first principles, of why certain combinations of dopants lead to particular results. This theoretical understanding will be essential in systematically tailoring the properties of SFO.

There have been several previous first-principles investigations of SFO. Fang et al investigated the electronic structure of SFO using density-functional theory (DFT)

* Corresponding author: kimg@ccs.msstate.edu

[21]. Park et al have calculated the exchange interaction of SFO from the differences of the total energy of different collinear spin configurations [22]. In spite of the importance of substituted SFO, only a few theoretical investigations have been done. Magnetism in La substituted SFO has been studied using DFT [23, 24]. The site occupancy and magnetic properties of Zn-Sn substituted SFO has been investigated [14].

In this work we use first-principles total-energy calculations to study the site occupation and magnetic properties of Al substituted *M*-type strontium hexaferrite $\text{SrFe}_{12-x}\text{Al}_x\text{O}_{19}$ with $x = 0.5$ and $x = 1.0$. Based on DFT calculations, we determine the the structure of various configurations of SFAO with different Al concentrations and compute the occupation probabilities for different substitution sites at elevated temperatures. We show that our model predicts an decrease of saturation magnetization as well as a decrease in magnetocrystalline anisotropy K_1 , and the increase of the anisotropy field H_a as the fraction of Al is increased, consistent with recent experimental measurements.

II. METHODS

SFO has a hexagonal magnetoplumbite crystal structure that belongs to $P63/mmc$ space group. Fig. 1 shows a unit cell of SFO used in the present work that contains 64 atoms of two formula units. Magnetism in SFO arises from Fe^{3+} ions occupying five crystallographically inequivalent sites in the unit cell, three octahedral sites ($2a$, $12k$, and $4f_2$), one tetrahedral site ($4f_1$), and one trigonal bipyramidal site ($2b$) as represented by the polyhedra in Fig. 1(a). SFO is also a ferrimagnetic material that has 16 Fe^{3+} ions with spins in the majority direction ($2a$, $2b$, and $12k$ sites) and 8 Fe^{3+} ions with spins in the minority direction ($4f_1$ and $4f_2$ sites) as indicated by the arrows in Fig. 1(b).

Total energies and forces were calculated using DFT with projector augmented wave (PAW) potentials as implemented in VASP [25, 26]. All calculations were spin polarized according to the ferrimagnetic ordering of Fe spins as first proposed by Gorter [21, 27]. A plane-wave energy cutoff of 520 eV was used both for pure SFO and Al-substituted SFO. Reciprocal space was sampled with a $7 \times 7 \times 1$ Monkhorst-Pack mesh [28] with a Fermi-level smearing of 0.2 eV applied through the Methfessel-Paxton method [29]. We performed relaxation of the electronic degrees of freedom until the change in free energy and the band structure energy was less than 10^{-7} eV. We performed geometric optimizations to relax the positions of ions and cell shape until the change in total energy between two ionic step was less than 10^{-4} eV. Electron exchange and correlation was treated with the generalized gradient approximation (GGA) as parameterized by the Perdew-Burke-Ernzerhof (PBE) scheme [30]. To improve the description of localized Fe $3d$ electrons, we employed the GGA+U method in the simplified rotationally

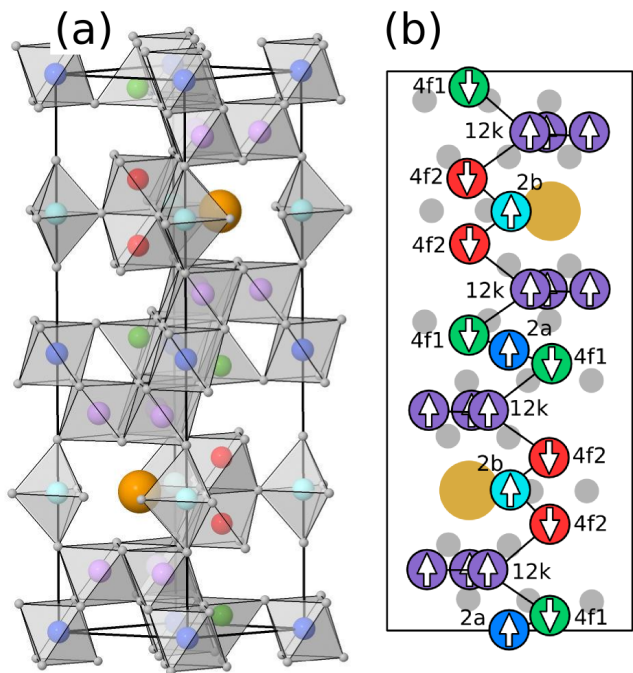


FIG. 1. (color online) (a) A unit cell of SFO containing two formula units. Two large gold spheres are Sr atoms and small gray spheres are O atoms. Colored spheres enclosed by polyhedra formed by O atoms represent Fe^{3+} ions in different inequivalent sites: $2a$ (blue), $2b$ (cyan), $12k$ (purple), $4f_1$ (green), and $4f_2$ (red). (b) A schematic diagram of the lowest-energy spin configuration of Fe^{3+} ions of SFO. The arrows represent the local magnetic moment at each atomic site. (For interpretation of the references to color in this figure caption, the reader is referred to the online version of this paper.)

invariant approach described by Dudarev et al [31]. This method requires an effective U value (U_{eff}) equal to the difference between the Hubbard parameter U and the exchange parameter J . We chose U_{eff} equal to 3.7 eV for Fe based on the previous result [14].

III. RESULTS AND DISCUSSION

The substitution of Fe^{3+} ions by Al^{3+} ions considerably affects the unit cell parameters. We have calculated the lattice parameters of pure and Al-substituted SFO by relaxing ionic positions as well as the volume and shape of the unit cell. In all cases the final unit cell was found to remain hexagonal. In the case of pure SFO, the lattice parameters a and c were found to be 5.93 Å and 23.21 Å in good agreement with the experimental values of $a = 5.88$ Å and $c = 23.04$ Å, respectively [19, 32]; the deviation between the experimental and the theoretical values is less than 1%. In the case of $x = 0.5$ in $\text{SrFe}_{12-x}\text{Al}_x\text{O}_{19}$ the lattice parameters a and c were calculated to be 5.92 Å and 23.16 Å respectively, while the volume of the unit cell was reduced by 0.61%. For

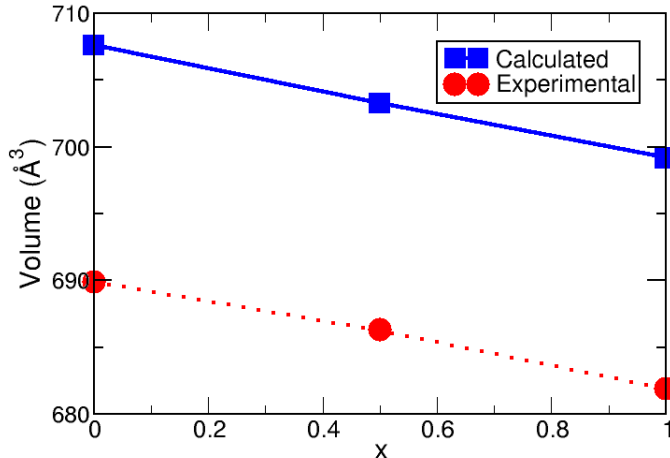


FIG. 2. (color online) Comparison of calculated and experimental (Ref. [19]) volume of the unit cell of $\text{SrFe}_{12-x}\text{Al}_x\text{O}_{19}$ as a function of the fraction of Al x .

$x = 1.0$, $a = 5.91 \text{ \AA}$ and $c = 23.04 \text{ \AA}$ were found, and reduction in the unit cell volume was 2.51%. Fig. 2 shows that the reduction of unit cell volume predicted by our DFT calculation is consistent with the experimental results [1, 19].

We investigated the site preference of Al substituting Fe in $\text{SrFe}_{12-x}\text{Al}_x\text{O}_{19}$ for (i) $x = 0.5$ and, (ii) $x = 1.0$. The $x = 0.5$ case corresponds to the condition where one Al atom is substituted in the unit cell, while two Al atoms were substituted in the case of $x = 1.0$ as shown Fig. 3. To determine the site preference of the substituted Al atoms, the substitution energy of configuration i was calculated using the following expression:

$$E_{\text{sub}}(i) = E(\text{SFAO}(i)) - E(\text{SFO}) - \sum_{\alpha} n_{\alpha} \epsilon(\alpha) \quad (1)$$

where $E(\text{SFAO}(i))$ is the total energy per unit cell at 0 K for SFAO in configuration i while $E(\text{SFO})$ is the total energy per unit cell at 0 K for SFO. $\epsilon(\alpha)$ is the total energy per atom for element α ($\alpha = \text{Al}, \text{Fe}$) at 0 K in its most stable crystal structure. n_{α} is the number of atoms of type α added: if two atoms are added then $n_{\alpha} = +2$ while $n_{\alpha} = -1$ when one atom is removed. The configuration with the lowest E_{sub} is concluded to be the ground state configuration, and the corresponding substitution site is the preferred site of Al atoms at 0 K.

To understand the site preference of the substituted Al^{3+} ions at higher temperatures, we compute the formation probability of configuration i using the Maxwell-Boltzmann statistical distribution [33]:

$$P_i = \frac{g_i \exp(-\Delta G_i/k_B T)}{\sum_j g_j \exp(-\Delta G_j/k_B T)} \quad (2)$$

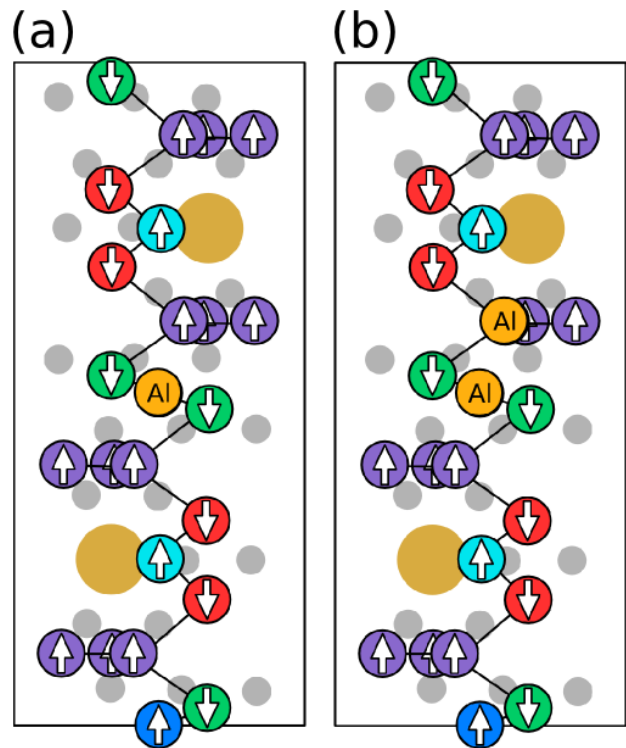


FIG. 3. (color online) The structures of $\text{SrFe}_{12-x}\text{Al}_x\text{O}_{19}$ with spins oriented in the easy axis (001): (a) configuration [2a] for $x = 0.5$ and (b) configuration [2a, 12k].1 for $x = 1.0$. Al atoms are labeled and other atoms are colored as in Fig. 1.

where g_i is the multiplicity of configuration i (number of equivalent configurations) and

$$\Delta G_i = \Delta E_{\text{sub}}(i) + P \Delta V_i - T \Delta S_i \quad (3)$$

is the change of the free energy of configuration i relative to that of the ground state configuration; $\Delta E_{\text{sub}}(i)$, ΔV_i , and ΔS_i are the substitution energy change, volume change, entropy change for configuration i ; P and k_B are the pressure and Boltzmann constant.

For the $x = 0.5$ concentration, one Al atom is substituted at one of the 24 Fe sites of the unit cell as shown in Fig. 3(a). The application of crystallographic symmetry operations shows that many of these Fe sites are equivalent and leaves only five inequivalent structures. We label these inequivalent configurations using the crystallographic name of the Fe site: [2a], [2b], [4f₁], [4f₂], and [12k]. These structures were created by substituting one Al atom to the respective Fe site of a SFO unit cell and performing full optimization of the unit cell shape and volume, and ionic positions.

Table I lists the results of our calculation for all five inequivalent configurations in the order of increasing substitution energy. The lowest E_{sub} is found for configuration [2a] shown in Fig. 1(a). We can conclude that at 0 K the most preferred site for the substituted Al atom is the 2a site. We used Eq. (2) to compute the

TABLE I. Five inequivalent configurations of $\text{SrFe}_{12-x}\text{Al}_x\text{O}_{19}$ with $x = 0.5$. g is the multiplicity of the configuration. E_{sub} is the substitution energy of the SFAO. The total magnetic moment (m_{tot}) and its change with respect to SFO (Δm_{tot}) are also given. All values are for a double formula unit cell containing 64 atoms. Energies are in eV while magnetic moments are in μ_{B} .

Config	g	E_{sub}	m_{tot}	Δm_{tot}
[2a]	2	-6.04	35	-5
[12k]	12	-6.00	35	-5
[4f ₂]	4	-5.63	45	+5
[2b]	2	-5.60	35	-5
[4f ₁]	4	-5.57	45	+5

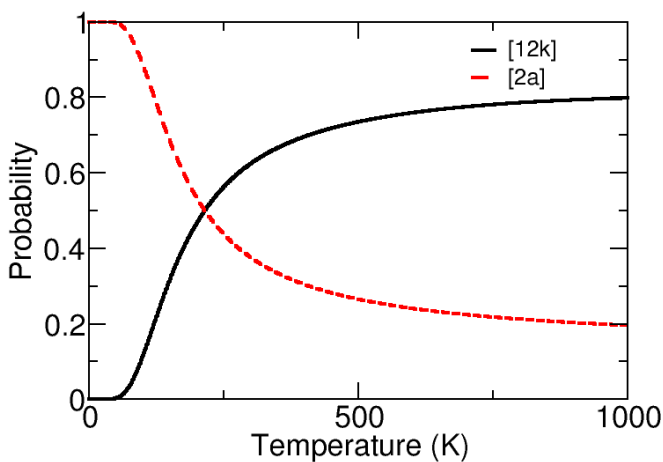


FIG. 4. (color online) Temperature dependence of the formation probability of different configurations of $\text{SrFe}_{12-x}\text{Al}_x\text{O}_{19}$ with $x = 0.5$. The configurations with negligible probability are not shown.

probability to form each configuration as a function of temperature. Since the volume change among different configurations is very small (less than 0.1 \AA^3), we can safely regard $P\Delta V$ term to be negligible (in the order of 10^{-7} eV at the standard pressure of 1 atm) compared to the $\Delta E_{\text{sub}}(i)$ term in Eq. (3). The entropy change ΔS has a configurational part, ΔS_c , and a vibrational part, ΔS_{vib} [34]. For binary substitutional alloys such as the present system, ΔS_{vib} is around 0.1-0.2 k_{B} /atom, and ΔS_c is 0.1732 k_{B} /atom [33]. Therefore, we set $\Delta S = 0.3732 k_{\text{B}}$ /atom.

Fig. 4 displays the temperature dependence of the formation probability of different configurations of $\text{SrFe}_{12-x}\text{Al}_x\text{O}_{19}$ with $x = 0.5$. The doped Al^{3+} ions mainly replace Fe^{3+} ions from the $2a$ and the $12k$ sites. The formation probabilities of [2b], [4f₁] and [4f₂] are negligible and not shown in Fig. 4. The probability that the doped Al^{3+} ion replaces Fe^{3+} ion from the $2a$ site is maximum at 0 K and it falls as temperature increases,

TABLE II. Ten lowest energy inequivalent configurations of $\text{SrFe}_{12-x}\text{Al}_x\text{O}_{19}$ with $x = 1.0$. g is the multiplicity of the configuration. E_{sub} is the substitution energy per Al atom. The total magnetic moment (m_{tot}) and its change with respect to SFO (Δm_{tot}) are also given. All values are for a double formula unit cell containing 64 atoms. Energies are in eV while moments are in μ_{B} .

Config	g	E_{sub}	m_{tot}	Δm_{tot}
[2a, 2a]	1	-6.056	30	-10
[2a, 12k].1	12	-6.054	30	-10
[2a, 12k].2	12	-6.041	30	-10
[12k, 12k].1	6	-6.025	30	-10
[12k, 12k].2	12	-6.025	30	-10
[12k, 12k].3	12	-6.027	30	-10
[12k, 12k].4	12	-6.025	30	-10
[12k, 12k].5	6	-6.023	30	-10
[12k, 12k].6	6	-6.017	30	-10
[12k, 12k].7	12	-6.014	30	-10

while the occupancy of Al^{3+} at the $12k$ site rises with temperature. The two curves cross at $T \sim 220$ K. At a typical annealing temperature of 1000 K for SFAO [1] the site occupation probability of the site $2a$ and $12k$ is 0.196 and 0.798, respectively. Thus, during the annealing process of the synthesis of the SFAO the doped Al^{3+} ions are more likely to replace Fe^{3+} ions from the $12k$ site than the $2a$ site despite of higher substitution energy.

For the $x = 1.0$ concentration, two Al atoms are substituted at two of the 24 Fe sites of the unit cell as shown in Fig. 3(b). These Fe sites have more than one equivalent site. Substitution of Al atoms breaks the symmetry of the equivalent sites of pure SFO. Out of all $C(24, 2) = 276$ possible structures, many of the structures are crystallographically equivalent. On applying crystallographic symmetry operations, the number of inequivalent structures reduces to 40. We label these inequivalent configurations using the convention of [(site for the first Al),(site for the 2nd Al)].(unique index). For example, when two Al atoms are substituted at the $2a$ and $12k$ sites, there are 2 inequivalent configurations, which are labeled as [2a, 12k].1 and [2a, 12k].2. These structures are fully optimized and their substitution energies are calculated using Eq. (1). When there are more than one inequivalent configuration, we assign the unique index in the order of increasing E_{sub} .

Table II lists the ten lowest energy configurations of $\text{SrFe}_{12-x}\text{Al}_x\text{O}_{19}$ with $x = 1.0$. The configuration [2a, 2a] where two Al^{3+} ions replace Fe^{3+} ions from two $2a$ sites has the lowest E_{sub} , and it is the most energetically favorable configuration at 0 K. To investigate the site occupation at nonzero temperatures we compute the formation probability of each configuration using Eq. (2). Similar to the previous case the volume change among different configurations is very small (less than 0.7 \AA^3) and we can safely ignore the $P\Delta V$ term. The entropy term is calculated in the same way as the $x = 0.5$ case. Fig. 5 shows the variation of the formation probability

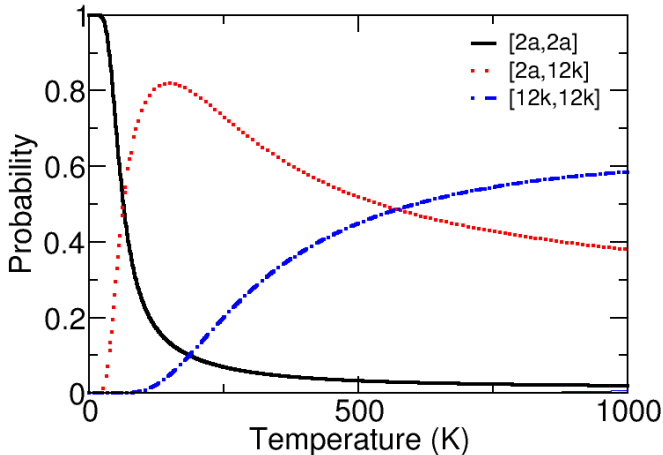


FIG. 5. (color online) Temperature dependence of the formation probability of different configurations of $\text{SrFe}_{12-x}\text{Al}_x\text{O}_{19}$ with $x = 1.0$. For clarity only the configurations with significant formation probability are labeled.

of different configurations with temperature. We note that due to low multiplicity of the configuration $[2a, 2a]$, its formation probability falls rapidly as temperature increases. On the other hand, the formation probability of the configuration $[2a, 12k]$ (sum of the formation probabilities for all $[2a, 12k].n$ configurations) increases steeply and reaches a maximum value at 50 K and then falls with temperature. Fig. 5 shows that the formation probability of the $[2a, 12k]$ configuration becomes larger than that of $[2a, 2a]$ beyond $T \sim 10$ K, which is a much lower transition temperature than in the $x = 0.5$ case.

We can calculate the occupation probability of Al at nonzero temperatures for a given site by adding all formation probabilities of the configurations where at least one Al^{3+} ion is substituted in that site. At the annealing temperature of 1000 K, the occupation probability of Al for 12k site is 79.8% for $x = 0.5$ as given in Table IV. The same probability is increased to 97.7% for $x = 1.0$ as calculated by adding the P_{1000} 's for all configurations that contain the 12k site. This means that the fraction of Al^{3+} ions occupying the 12k site increases when the fraction of Al is increased from $x = 0.5$ to $x = 1.0$. This conclusion is in agreement with the previously reported measurements [1, 16, 35].

In Table III we compare the contribution of different sublattices to the total magnetic moment in Al-substituted SFO. To see the effect of Al^{3+} ions in different substitution sites, we split the entries of sublattices containing these ions ($2a$ and $12k$). As expected, Al^{3+} ions carry negligible magnetic moment regardless of their substitution sites. Consequently, when they replace Fe^{3+} ions in the minority spin sites ($4f_1$ and $4f_2$), they eliminate a negative contribution and hence increase the total magnetic moment. On the other hand, when they re-

place Fe^{3+} ions in the majority spin sites ($12k$, $2a$, and $2b$), they eliminate a positive contribution and hence reduce the total magnetic moment. For the $x = 0.5$ case, the most probable sites are $12k$ and $2a$ (majority sites) and the net magnetic moment of the unit cell is reduced by $5 \mu_B$. For the configuration $[2a, 12k].1$ of the $x = 1.0$ case, two Al atoms are substituted in the $2a$ and $12k$ sites, there is a reduction of $10 \mu_B$ in the total magnetic moment per unit cell.

Magnetic Anisotropy determines the capacity of a magnet to withstand external magnetic and electric fields. This property is of considerable practical interest, because anisotropy is exploited in the design of the most magnetic materials of commercial importance. The magnetocrystalline anisotropy energy (MAE) is one of the main factors that determine the total magnetic anisotropy of the material. To investigate the effect of Al substitution on the magnetic anisotropy of SFO, we computed the MAE and the magnetic anisotropy constant of $\text{SrFe}_{12-x}\text{Al}_x\text{O}_{19}$ for $x = 0, 0.5$ and 1. The MAE, in the present case, is defined as the difference between the two total energies where electron spins are aligned along two different directions [36]:

$$E_{\text{MAE}} = E_{(100)} - E_{(001)} \quad (4)$$

where $E_{(100)}$ is the total energy with spin quantization axis in the magnetically hard plane and $E_{(001)}$ is the total energy with spin quantization axis in the magnetically easy axis. Using the MAE, the uniaxial magnetic anisotropy constant K_1 can be computed [37, 38]

$$K_1 = \frac{E_{\text{MAE}}}{V \sin^2 \theta} \quad (5)$$

where V is the equilibrium volume of the unit cell and θ is the angle between the two spin quantization axis orientations (90° in the present case). The anisotropy field H_a can be expressed as [39]

$$H_a = \frac{2K_1}{M_s} \quad (6)$$

where K_1 is a magnetocrystalline anisotropy constant and M_s is saturation magnetization.

The results for the MAE, the magnetocrystalline anisotropy constant K_1 , and anisotropy field H_a for SFAO with different Al concentration are presented in Table IV. To compare with experimental results, we also compute the weighted average of K_1 and H_a using the formation probability P_{1000} at a typical annealing temperature of 1000 K [1]. We note that SFAO considered in the present work loses most of its magnetic properties at typical annealing temperatures (1000 K or higher) that are near or above its Curie temperature. The magnetic properties listed in Table IV refer to their ground state properties at the temperature $T = 0$. We use the formation probability at 1000 K to compute the weighted averages as the crystalline configurations of SFAO will be

TABLE III. Contribution of atoms in each sublattice to the total magnetic moment of Al-substituted SFO structures [12*k*], [2*a*], and [2*a*, 12*k*].1 compared with pure SFO. All magnetic moments are in μ_B . Δm is measured relative to the values for the pure SFO. Note that the total magnetic moment of the unit cell (m_{tot}) is slightly different than the sum of local magnetic moments due to the contribution from the interstitial region.

site	SFO		[12 <i>k</i>]			[2 <i>a</i>]			[2 <i>a</i> , 12 <i>k</i>].1		
	atoms	<i>m</i>	atoms	<i>m</i>	Δm	atoms	<i>m</i>	Δm	atoms	<i>m</i>	Δm
2 <i>d</i>	2 Sr	-0.006	2 Sr	-0.006	0.000	2 Sr	-0.006	0.000	2 Sr	-0.006	0.000
2 <i>a</i>	1 Fe	4.156	1 Fe	4.155	-0.001	1 Al	-0.010	-4.166	1 Al	-0.010	-4.166
	1 Fe	4.156	1 Fe	4.156	0.000	1 Fe	4.156	0.000	1 Fe	4.156	0.000
2 <i>b</i>	2 Fe	8.098	2 Fe	8.086	-0.012	2 Fe	8.100	0.001	2 Fe	8.090	-0.008
4 <i>f</i> ₁	4 Fe	-16.152	4 Fe	-16.189	-0.037	4 Fe	-16.268	-0.116	4 Fe	-16.304	-0.152
4 <i>f</i> ₂	4 Fe	-16.384	4 Fe	-16.420	-0.036	4 Fe	-16.382	0.002	4 Fe	-16.418	-0.034
12 <i>k</i>	1 Fe	4.172	1 Al	0.000	-4.172	1 Fe	4.170	-0.002	1 Al	-0.001	-4.173
	11 Fe	45.884	11 Fe	45.861	-0.023	11 Fe	45.872	-0.012	11 Fe	45.846	-0.038
4 <i>e</i>	4 O	1.416	4 O	1.304	-0.112	4 O	1.424	0.008	4 O	1.316	-0.100
4 <i>f</i>	4 O	0.360	4 O	0.281	-0.079	4 O	0.310	-0.050	4 O	0.230	-0.129
6 <i>h</i>	6 O	0.124	6 O	0.115	0.009	6 O	0.134	0.010	6 O	0.117	-0.007
12 <i>k</i>	12 O	1.016	12 O	0.877	-0.129	12 O	0.548	-0.468	12 O	0.404	-0.612
12 <i>k</i>	12 O	2.140	12 O	1.895	-0.245	12 O	2.088	-0.052	12 O	1.839	-0.301
$\sum m$		38.980		34.114	-4.837		34.136	-4.845		29.259	-9.720
m_{tot}		40		35	-5		35	-5		30	-10

TABLE IV. The saturation magnetization (M_s), magnetocrystalline anisotropy energy (MAE), magnetocrystalline anisotropy constant (K_1) and anisotropy field (H_a) for SFO and SFAO. x is the Al fraction in $\text{SrFe}_{12-x}\text{Al}_x\text{O}_{19}$ and V is the volume of the unit cell in \AA^3 . P_{1000} is the formation probability at 1000 K. The averaged quantities are weighted by P_{1000} . M_s is in emu/g, MAE in meV, H_a in kOe, and K_1 in $\text{kJ}\cdot\text{m}^{-3}$.

x	Config	M_s	MAE	V	K_1	H_a	P_{1000}	$\langle M_s \rangle$	$\langle K_1 \rangle$	$\langle H_a \rangle$
0.0	SFO	110.19	0.85	707.29	193	7.35	1.000	110.19	193	7.35
0.5	[2 <i>a</i>]	96.41	0.95	703.29	216	9.38	0.196	96.49	189	8.18
	[12 <i>k</i>]	96.41	0.80	703.19	182	7.90	0.798			
	[2 <i>b</i>]	96.41	0.67	702.82	152	6.62	0.003			
	[4 <i>f</i> ₁]	123.96	0.86	704.22	196	6.61	0.001			
	[4 <i>f</i> ₂]	123.96	0.83	702.58	189	6.38	0.001			
1.0	[2 <i>a</i> , 2 <i>a</i>]	82.64	0.99	698.94	227	11.41	0.019	83.03	184	9.23
	[2 <i>a</i> , 12 <i>k</i>]	82.64	0.88	699.08	202	10.13	0.379			
	[12 <i>k</i> , 12 <i>k</i>]	82.64	0.75	698.66	172	8.64	0.585			
	[12 <i>k</i> , 4 <i>f</i> ₂]	110.19	0.78	690.64	181	6.74	0.007			
	[12 <i>k</i> , 4 <i>f</i> ₁]	110.19	0.80	700.29	183	6.92	0.004			
	[12 <i>k</i> , 2 <i>b</i>]	82.64	0.62	698.98	142	7.14	0.002			
	[4 <i>f</i> ₂ , 4 <i>f</i> ₂]	137.74	0.80	697.96	184	5.53	0.000			
	[4 <i>f</i> ₂ , 4 <i>f</i> ₁]	137.74	0.83	699.62	191	5.74	0.000			
	[4 <i>f</i> ₂ , 2 <i>b</i>]	110.19	0.60	698.82	138	5.19	0.000			
	[4 <i>f</i> ₂ , 2 <i>a</i>]	110.19	0.90	698.53	206	7.78	0.002			
	[4 <i>f</i> ₁ , 4 <i>f</i> ₁]	137.74	0.86	701.38	196	5.95	0.000			
	[4 <i>f</i> ₁ , 2 <i>b</i>]	110.19	0.65	699.95	149	5.62	0.000			
	[4 <i>f</i> ₁ , 2 <i>a</i>]	110.19	0.91	700.11	208	7.87	0.001			
	[2 <i>b</i> , 2 <i>b</i>]	82.64	0.45	698.86	103	5.19	0.000			
[2 <i>b</i> , 2 <i>a</i>]	82.64	0.74	698.82	170	8.53	0.001				

distributed according to this value during the annealing process.

Table IV shows that M_s decreases as the concentration of Al x is increased from 0 to 0.5 to 1.0, consistent with the previous experimental results [1, 20, 40, 41]. Our calculation also shows that K_1 decreases as the concentration of Al x is increased from 0 to 0.5 to 1.0. At a low temperature Al atoms prefer to occupy the 2*a* sites,

which would have increased K_1 (see K_1 values for [2*a*] and [2*a*, 2*a*] in Table IV). However, the formation probability of the configurations involving 12*k* site (such as [12*k*], [2*a*, 12*k*] and [12*k*, 12*k*]) increases significantly as the temperature rises due to the entropy contribution of the free energy. At the annealing temperature Al³⁺ ions are much more likely to occupy the 12*k* site than the 2*a* site. This causes the magnetocrystalline anisotropy con-

stant K_1 of Al-substituted SFO to be reduced with the increase of Al fraction x , consistent with the experimental measurement reported by Albanes [40]. Despite of this, M_s is reduced more significantly than K_1 and this causes the anisotropy field H_a in Eq. (6) to increase as the concentration of Al x is increased from 0 to 0.5 to 1.0 as shown in Table IV. This result is consistent with several experimental results [1, 41].

IV. CONCLUSIONS

Using the first-principles total energy calculations based on density functional theory, we obtained the ground state structures and associated formation probabilities at finite temperatures for Al-substituted SFO, $\text{SrFe}_{12-x}\text{Al}_x\text{O}_{19}$ with $x = 0.5$ and 1.0 . The structures derived from our calculations show that the total magnetic moment of the SFO unit cell is reduced as the fraction of Al atoms increases. This reduction of magnetization is explained by the fact that the non-magnetic Al atoms prefer to replace Fe^{3+} ions at two of the majority spin sites, $2a$ and $12k$, eliminating their positive contribution

to the total magnetization. Our model also explains the increase of the observed anisotropy field when the fraction of Al in SFO is increased. At the annealing temperature Al^{3+} ions are much more likely to occupy the $12k$ site than the $2a$ site. Although this causes the magnetocrystalline anisotropy to decrease slightly, the reduction in the saturation magnetization is larger and their combined effect causes the magnetic anisotropy field of Al-substituted SFO to be reduced with increase of Al fraction x . Our results are consistent with the available experimental measurement on Al-substituted SFO.

V. ACKNOWLEDGMENTS

This work was supported in part by the U.S. Department of Energy ARPA-E REACT program under Award Number de-ar0000189 and the Center for Computational Science (CCS) at Mississippi State University. Computer time allocation has been provided by the High Performance Computing Collaboratory (HPC²) at Mississippi State University.

-
- [1] H. Wang, B. Yao, Y. Xu, Q. He, G. Wen, S. Long, J. Fan, G. Li, L. Shan, B. Liu, L. Jiang, and L. Gao, *Journal of Alloys and Compounds* **537**, 43 (2012).
 - [2] R. C. Pullar, *Progress in Materials Science* **57**, 1191 (2012).
 - [3] Z. Pang, X. Zhang, B. Ding, D. Bao, and B. Han, *Journal of Alloys and Compounds* **492**, 691 (2010).
 - [4] A. Davoodi and B. Hashemi, *Journal of Alloys and Compounds* **509**, 5893 (2011).
 - [5] M. N. Ashiq, M. J. Iqbal, M. Najam-ul Haq, P. Hernandez Gomez, and A. M. Qureshi, *Journal of Magnetism and Magnetic Materials* **324**, 15 (2012).
 - [6] D. Seifert, J. Tpfers, F. Langenhorst, J.-M. L. Breton, H. Chiron, and L. Lechevallier, *Journal of Magnetism and Magnetic Materials* **321**, 4045 (2009).
 - [7] J. Wang, C. Ponton, R. Grössinger, and I. Harris, *Journal of Alloys and Compounds* **369**, 170 (2004).
 - [8] J. Wang, C. Ponton, and I. Harris, *Journal of Magnetism and Magnetic Materials* **234**, 233 (2001).
 - [9] J. Wang, C. Ponton, and I. Harris, *Journal of Alloys and Compounds* **403**, 104 (2005).
 - [10] J. Wang, C. Ponton, and I. Harris, *IEEE Transactions on Magnetics* **38**, 2928 (2002).
 - [11] Q. Fang, *Journal of Applied Physics* **95**, 6360 (2004).
 - [12] A. Ghasemi, V. Šepelák, X. Liu, and A. Morisako, *Journal of Applied Physics* **107**, 09A734 (2010).
 - [13] A. Ghasemi and V. Šepelák, *Journal of Magnetism and Magnetic Materials* **323**, 1727 (2011).
 - [14] L. S. Liyanage, S. Kim, Y.-K. Hong, J.-H. Park, S. C. Erwin, and S.-G. Kim, *Journal of Magnetism and Magnetic Materials* **348**, 75 (2013).
 - [15] W. Liu, H. Sun, X. Yi, X. Liu, D. Zhang, M. Yue, and J. Zhang, *Journal of Alloys and Compounds* **501**, 67 (2010).
 - [16] E. Bertaut, A. Deschamps, R. Pauthenet, and S. Pickart, *J. Phys. Radium* **20**, 404 (1959).
 - [17] S. Wang, J. Ding, Y. Shi, and Y. Chen, *Journal of Magnetism and Magnetic Materials* **219**, 206 (2000).
 - [18] M. Liu, X. Shen, F. Song, J. Xiang, and X. Meng, *Journal of Solid State Chemistry* **184**, 871 (2011).
 - [19] H. Luo, B. Rai, S. Mishra, V. Nguyen, and J. Liu, *Journal of Magnetism and Magnetic Materials* **324**, 2602 (2012).
 - [20] I. Harward, Y. Nie, D. Chen, J. Baptist, J. M. Shaw, E. Jakubisov Likov, . Viovsk, P. irok, M. Lesk, J. Pitora, and Z. Celinski, *Journal of Applied Physics* **113**, 043903 (2013).
 - [21] C. Fang, F. Kools, R. Metselaar, R. Groot, and Others, *Journal of Physics: Condensed Matter* **15**, 6229 (2003).
 - [22] J. Park, Y.-K. Hong, S.-G. Kim, S. Kim, L. S. Liyanage, J. Lee, W. Lee, G. S. Abo, K.-H. Hur, and S.-Y. An, *Journal of Magnetism and Magnetic Materials* **355**, 1 (2014).
 - [23] M. Küpferling, P. Novák, K. Knížek, M. W. Pieper, R. Grössinger, G. Wiesinger, and M. Reissner, *Journal of Applied Physics* **97**, 10F309 (2005).
 - [24] P. Novk, K. Knek, M. Kpferling, R. Grssinger, and M. W. Pieper, *The European Physical Journal B - Condensed Matter and Complex Systems* **43**, 509 (2005), 10.1140/epjb/e2005-00084-8.
 - [25] G. Kresse and J. Furthmüller, *Phys. Rev. B* **54**, 11169 (1996).
 - [26] G. Kresse and D. Joubert, *Phys. Rev. B* **59**, 1758 (1999).
 - [27] E. F. Gorter, *Proc. IEEE* **104B**, 2555 (1957).
 - [28] H. Monkhorst and J. Pack, *Phys. Rev. B* **13**, 5188 (1976).
 - [29] M. Methfessel and A. T. Paxton, *Phys. Rev. B* **40**, 3616 (1989).

- [30] J. P. Perdew, K. Burke, and M. Ernzerhof, *Phys. Rev. Lett.* **77**, 3865 (1996).
- [31] S. L. Dudarev, G. A. Botton, S. Y. Savrasov, C. J. Humphreys, and A. P. Sutton, *Phys. Rev. B* **57**, 1505 (1998).
- [32] K. Kimura, M. Ohgaki, K. Tanaka, H. Morikawa, and F. Marumo, *Journal of Solid State Chemistry* **87**, 186 (1990).
- [33] X. B. Liu, Y. Ma, Z. Altounian, Q. Zhang, and J. Ping Liu, *Journal of Applied Physics* **115**, 17A702 (2014).
- [34] A. van de Walle and G. Ceder, *Rev. Mod. Phys.* **74**, 11 (2002).
- [35] G. Albanese, *Journal of Magnetism and Magnetic Materials* **147**, 421 (1995).
- [36] P. Ravindran, A. Delin, P. James, B. Johansson, J. M. Wills, R. Ahuja, and O. Eriksson, *Phys. Rev. B* **59**, 15680 (1999).
- [37] F. Muñoz, A. Romero, J. Mejía-López, and J. Morán-López, *Journal of Nanoparticle Research* **15**, 1524 (2013), 10.1007/s11051-013-1524-6.
- [38] J. Smit and H. Wijn, *Ferrites* (Philips Technical Library, Eindhoven, 1959).
- [39] C. Kittel, *Rev. Mod. Phys.* **21**, 541 (1949).
- [40] G. Albanese and A. Deriu, *Ceramurgia International* **5**, 3 (1979).
- [41] A. B. Ustinov, A. S. Tatarenko, G. Srinivasan, and A. M. Balbashov, *Journal of Applied Physics* **105**, 023908 (2009).